Product Branching Fractions and Kinetic Isotope Effects for the Reactions of OH and OD Radicals with CH_3SH and CH_3SD

N. I. Butkovskaya[†] and D. W. Setser*[,‡]

Institute of Chemical Physics, Russian Academy of Sciences, 117334 Moscow, Russian Federation, and Kansas State University, Department of Chemistry, Manhattan, Kansas, 66506

Received: May 5, 1999; In Final Form: July 7, 1999

Product branching fractions and kinetic isotope effects for the reactions of OH and OD radicals with CH_3SH and CH_3SD were determined from the infrared chemiluminescent spectra of the H_2O, HDO and D_2O products. The spectra were acquired by a Fourier transform spectrometer that viewed the emission from a discharge flow reactor. Abstraction of H atom from the methyl group accounts for (11 ± 4)% of the total reaction rate from the OD + CH_3SD (or OD + CH_3SH) reaction and for (24 ± 8)% from the OH + CH_3SH (or OH + CH_3SD) reaction. The major product channel involves interaction with the sulfur end of the molecule. The difference in branching fractions for OD and OH reactions is due to the large inverse secondary kinetic-isotope effect for the addition−elimination channel, which occurs by transfer of the hydrogen atom from the sulfur atom to the oxygen atom in the adduct. Transition state models for the elimination channel are discussed to show that the experimentally determined secondary kinetic isotope effect for the addition−elimination step, $k_{OH}/k_{OD} = 0.6 \pm 0.1$, obtained from the intensity ratios is reasonable. The basis spectra used for simulation of the $\Delta\nu_3 = -1$ emission spectra of D_2O were refined, relative to previous work, and the improvements are described in the Appendix.

1. Introduction

The reaction with OH radicals is the initial step for the oxidation of methanethiol, CH_3SH, in the troposphere, and a knowledge of the products is necessary before the secondary reactions that lead to the end products can be formulated. This reaction has been a subject of a number of kinetic studies,[1−6] which were summarized in the review of Tyndall and Ravishankara [1]. A negative temperature dependence in the 244−430 K range has been established for the rate constant with $k_{298} = (3.3 \pm 0.4) \times 10^{-11}$ cm^3 molecule^{-1} s^{-1} and $E_a = -0.7 \pm 0.2$ kcal mol^{-1}. The CH_3S yield from the OH + CH_3SH reaction was estimated[2] to be 1.1 ± 0.2, which led to the conclusion that (1a) is the main reaction.

$$OH + CH_3SH \rightarrow CH_3S + H_2O \qquad (1a)$$

The mechanism is thought to proceed by way of a $CH_3S(OH)H$ intermediate. This addition mechanism was initially supported by the absence of a significant kinetic-isotope effect for reactions of OH with CH_3SD and CD_3SH.[3,4]

In our recent work using infrared Fourier transform chemiluminescent spectroscopy,[7] we observed the water molecules produced by the OH and OD + CH_3SH reactions. The available energy, 34 kcal mol^{-1}, is sufficient to excite up to three stretching quanta in the water molecule. The H_2O and HOD vibrational distributions obtained from the infrared chemiluminescent spectra differed from those associated with direct abstraction reactions, and they were more typical of water addition−elimination reactions. However, we could not entirely exclude the possibility that a part of the reaction occurs with the CH_3 group, either from the adduct or by direct abstraction. Reaction 1b is exothermic by 26 kcal mol^{-1},

$$OH + CH_3SH \rightarrow CH_2SH + H_2O \qquad (1b)$$

which allows excitation up to two stretching quanta in the H_2O molecule. In our previous study, channels a and b could not be separated for either reaction 1 or for its OD isotopic analogue.

$$OD + CH_3SH \rightarrow CH_3S + HOD \qquad (2a)$$

$$\rightarrow CH_2SH + HOD \qquad (2b)$$

The reaction with dimethyl sulfide (DMS),

$$OH\ (OD) + CH_3SCH_3 \rightarrow CH_2SCH_3 + H_2O\ (HOD) \qquad (3)$$

with a rate constant[1], $k_{298} = (4.4 \pm 0.4) \times 10^{-12}$ cm^3 molecule^{-1} s^{-1}, proceeds by direct abstraction for low-pressure conditions and gives an inverted distribution in the H_2O(HOD) stretch modes.[7] Even if the $CH_3S(OH)H$ adduct does not eliminate a hydrogen from the CH_3 group, direct abstraction would be expected to make a 5−10% contribution to reactions 1 and 2.

In the present work, the infrared chemiluminescence from the reactions of OH and OD radicals with CH_3SD was observed and recorded using the same technique as used for reactions 1 and 2.[7]

$$OH + CH_3SD \rightarrow HOD + CH_3S \qquad (4a)$$

$$\rightarrow H_2O + CH_2SD \qquad (4b)$$

and

$$OD + CH_3SD \rightarrow D_2O + CH_3S \qquad (5a)$$

$$\rightarrow HOD + CH_2SD \qquad (5b)$$

[†] Russian Academy of Sciences.
[‡] Kansas State University.

10.1021/jp9914828 CCC: $18.00
Published on Web 08/17/1999

The H_2O, HOD, and D_2O spectra in the 2400−4200 cm^{-1} range for reactions 1, 2, 4, and 5 were acquired under conditions such that vibrational relaxation does not occur (except for the collisionally coupled levels[7]). The vibrational distributions for all three isotopic water molecules were assigned from these spectra by computer simulation following the methods described previously.[7−10]

The reaction of OH and OD radicals with dimethyl disulfide (DMDS) gave infrared emission spectra that were identical to those from reactions 1 and 5, respectively.[8] Analysis of the kinetic behavior of the observed emission showed that the primary reactions proceed with formation of CH_3SH or CH_3SD molecules, and that the observed H_2O and D_2O spectra were due to the secondary reactions with CH_3SH or CH_3SD. Thus, the OD + DMDS system could be used as a clean source of CH_3SD. Having spectra from both OD + DMDS and OD + CH_3SD, we could estimate the isotopic purity of the CH_3SD in the reactor. Comparison of the measured D_2O and HOD integrated spectral intensities for reactions 5a and 5b, respectively, confirmed that the reaction is dominated by channel 5a with a branching fraction for channel 4b of about 11%. The HOD and H_2O intensities observed from reactions 4a and 4b gave a branching fraction for reaction 4b of about 24%.

The measured branching fractions are related to the kinetic-isotope effects (KIE) for the set of reactions under study. These isotope effects were obtained from the integrated emission intensities and using the ratio of emission probabilities for H_2O, HOD, and D_2O with estimation of the fraction of molecules that are formed in levels which do not emit. The H_2O and HOD yields, as deduced from the intensities from reactions 1 and 2, respectively, correspond to an inverse secondary KIE $k_{OH}/k_{OD} = 0.67 \pm 0.11$. Comparison of the emission intensities of HOD and D_2O from reactions 4 and 5 gave a secondary KIE specifically for channel b, $k_{OH}/k_{OD} = 0.60 \pm 0.05$, which will be discussed from the point of view of transition state theory.

Our first attempt to model D_2O emission spectra was reported in a study of the OD + DBr reaction;[9] the rigid rotor approximation was used to calculate the rotational line strengths, and a conventional spectroscopic expression with anharmonicities was used to calculate the vibrational energy levels. To increase the reliability of the simulation, more precise intensities for the transitions in the fundamental emission bands were calculated in the present work, using the expansion of the transformed dipole moment. Details of the calculations for simulation of the D_2O spectra are given in the Appendix.

2. Experimental and Computational Techniques

2.1. Experimental Methods. The experimental apparatus and procedures have been described in several preceding papers.[7−10] The infrared chemiluminescence spectra from vibrationally excited H_2O, HOD, and D_2O molecules from the reactions of OH and OD radicals with CH_3SH and CH_3SD were recorded by a Fourier transform infrared spectrometer (BIORAD), which viewed the fast-flow reactor through a NaCl window. Each measured spectrum represents an average of 512 scans of the spectrometer with a spectral resolution of 2 cm^{-1}. A SPECTROGON SP-4300 nm filter was installed in front of the detector, which reduced the noise level compared to spectra from the previous study.[7] The OH or OD radicals were produced via the reaction of H or D with NO_2 in the prereactor section of the flow reactor. The H or D atoms were generated by a microwave discharge in $H_2(D_2)$/Ar mixtures. The CH_3SH or CH_3SD was introduced into the reactor through a ring injector located 20 cm downstream of the hydrogen and nitrogen dioxide inlets and 3.5 cm upstream of the observation window. For a total pressure of about 0.5 Torr, the flow velocity was about 140 m s^{-1}, corresponding to a reaction time of $\Delta t \approx 0.2$ ms. The concentration of H or D atoms was in the range of $(2-4) \times 10^{13}$ molecules cm^{-3}; the NO_2 concentration was maintained between 4 and 10×10^{13} molecules cm^{-3}; the methanethiol reactant concentrations were varied from 2×10^{13} to 6×10^{13} molecules cm^{-3}. The flow rates and pressures were measured as described previously.

Commercial tank grade Ar passed through three molecular sieve traps cooled by either an acetone/dry ice mixture or liquid N_2 for purification. The CH_3SD (CDN Isotopes, Canada) was stored as 20% mixture in Ar in a 10 L glass reservoir which had been treated with D_2O and pure CH_3SD before the mixture was prepared. The inlet glass lines and the reactor were treated by a CH_3SD flow for ∼1/2 h before each experiment. The isotopic and chemical purity of CH_3SD were stated to be >94% and >99.6%, respectively. The CH_3SH contamination in CH_3SD in the reactor (which can include H/D exchange in the lines) was estimated spectroscopically by comparison with the spectra from OD + CH_3SSCH_3 reaction to be about 3% (see below).

2.2. Modeling of H_2O, HOD, and D_2O Spectra. Earlier,[7−10] we showed that H_2O and HOD spectra obtained from experiments at <0.7 Torr and Δt < 0.35 ms were not affected by vibrational relaxation, but the ν_1 and ν_3 modes in H_2O and the ν_1 and $2\nu_2$ modes in HOD are collisionally equilibrated so that only the combined distribution can be assigned for the $\nu_{1,3}$ and $\nu_{1,2}$ reservoirs, respectively. Such equilibration occurs because of the close energies of the (ν_1,ν_2,ν_3) and $(\nu_1 + 1, \nu_2, \nu_3 - 1)$ levels of H_2O and (ν_1, ν_2, ν_3) and $(\nu_1 + 1, \nu_2 - 2, \nu_3)$ levels of HOD. Accordingly, the reservoir distributions are assigned to the quantum numbers $\nu_{1,3} = \nu_1 + \nu_3$ and ν_2 in the case of H_2O, and $\nu_{1,2} = \max \nu_2$ in the set of close levels with the same ν_3 in the case of HOD. Similar equilibration between the ν_1 and ν_3 modes occurs for D_2O. Furthermore, the density of vibrational levels of D_2O is higher than for H_2O, and some energy exchange can take place between different $\nu_{1,3}$ manifolds; this D_2O relaxation is discussed in section 3.2.

The procedure for computer simulation of the H_2O and HOD spectra was fully described[7−10] when the vibrational distributions for H_2O and HOD from reactions 1 and 2 were presented.[7] The simulation method is based on calculation of the H_2O and HOD fundamental emission bands for a 300 K Boltzmann rotational population from the known ν_1, $2\nu_2$, and ν_3 absorption bands, assuming a cubic dependence of the emission intensity upon the transition frequency. The error analysis associated with the least-squares fitting showed[7] that the main error in the vibrational populations is connected with determination of the populations in the "dark" vibrational states, namely, the $20\nu_20$ states ($\nu_{1,3} = 0$) of H_2O and 000 and 010 states of HOD.

Calculation of the fundamental ν_1 and ν_3 emission bands of D_2O is described in the Appendix. The D_2O spectra were fitted by red-shifting these fundamentals bands, as previously described, but using band centers for higher vibrational levels that were determined from experiments.[11,12] For band centers that have not been measured, it was necessary to use calculations,[13] and the positions of bands with $\nu_2 \geq 5$ were estimated by extrapolation.

3.Results and Discussion

3.1. Chemiluminescent Spectra and Vibrational Distributions. The raw chemiluminescent spectra from the four reactions are shown in Figure 1; all spectra have been normalized to the intensity of the highest peak. The spectrum from the OH +

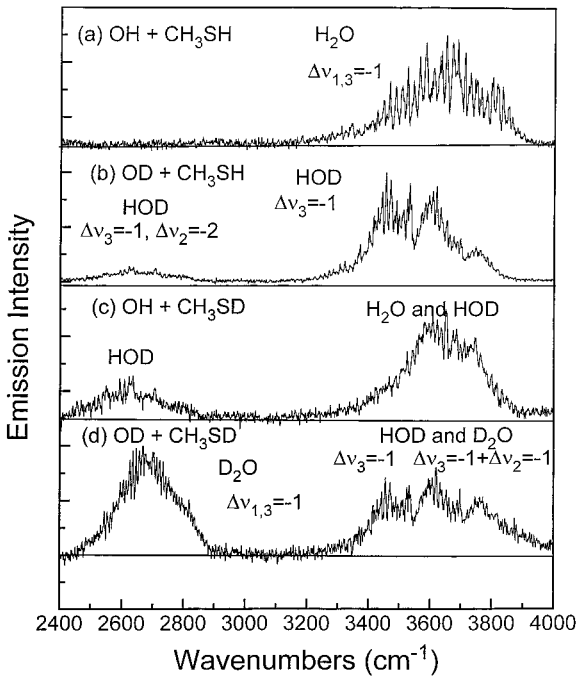

Figure 1. Raw chemiluminescent spectra from reactions of hydroxyl radicals with methanethiol at 0.5 Torr ($\Delta t \simeq 0.25$ ms) and [OH] = [OD] = 2×10^{13}, [NO_2] $\approx 1 \times 10^{14}$, and [CH_3SH] $\approx$ [CH_3SD] $\approx 6 \times 10^{13}$ molecules cm^{-3}: (a) OH + CH_3SH; (b) OD + CH_3SH; (c) OH + CH_3SD; (d) OD + CH_3SD.

TABLE 1: Vibrational Distribution of H_2O from the Reaction of OH with CH_3SH and CH_3SCH_3 and D_2O from the Reaction of OD with CH_3SD

	ν_2										
$\nu_{1,3}$[a]	0	1	2	3	4	5	6	7	$P_{1,3}$[b]	$P_{1,3}$[c]	$P_{1,3}^0$
					H_2O (OH + CH_3SH)						
0										44.2	52.6
1	19.1	24.8	14.2	8.5	2.4				69.1	38.5	35.2
2	15.4	11.4	0.8						27.6	15.5	11.5
3	3.3								3.3	1.8	0.7
					H_2O (OH + CH_3SCH_3)[d]						
0										28.2	63.2
1	20.4	26.7	13.1	6.3					66.5	47.7	32.2
2	21.5	12.0							33.5	24.0	4.6
					D_2O (OD + CH_3SD)						
0										30.0	35.9
1	14.8	13.7	8.8	5.8	9.6	6.0	3.0	3.4	65.1	43.0	34.3
2	9.6	4.2	7.0	2.6	8.2				31.6	24.5	20.7
3	1.5	0.6	1.2						3.3	2.5	7.5
4	0.8										

[a] $\nu_{1,3} = \nu_1 + \nu_3$. [b] $P_{1,3}(0)$ is disregarded. [c] $P_{1,3}(0)$ as obtained from the linear surprisal plot for H_2O distributions and as estimated from comparison with the presented H_2O distribution from CH_3SH reaction for D_2O (see text); $P_{1,3}^0$ is the statistical distribution [d] The distribution from the CH_3SCH_3 reaction was taken from ref 7.

CH_3SH reaction in Figure 1a consists of the $\Delta\nu_3 = -1$ and $\Delta\nu_1 = -1$ transitions from the collisionally coupled ν_1 and ν_3 levels of H_2O. The very weak overtone $\Delta\nu_2 = -2$ transitions of H_2O, which also fall into the 3200−3900 cm^{-1} range, can be neglected. The stretching distribution $P_{1,3}(0:1:2:3)$ is 44:39:16:2, as previously determined,[7] with $P_{1,3}(0)$ assigned from the linear surprisal plot extrapolation (see Table 1). The HOD molecules from OD + CH_3SH emit in two spectral ranges as shown in Figure 1b: the 3200−3900 cm^{-1} range corresponds to $\Delta\nu_3 = -1$ transitions, and the 2400−2900 cm^{-1} range corresponds to the $\Delta\nu_1 = -1$ and $\Delta\nu_2 = -2$ transitions from the collisionally coupled ν_1 and ν_2 excited states including

TABLE 2: Vibrational Distributions of HOD from the Reactions of OD with CH_3SH and CH_3SCH_3 and OH with CH_3SD

	$\nu_{1,2}$									
ν_3	0	1	2	3	4	5	6	7	P_3	P_3^0
				OD + CH_3SH						
0	12.7[a]	8.5[a]	12.7	8.5	2.9	2.3	2.6	2.1	52.3	74.8
1	12.1	3.7	6.7	1.7	1.2	0.3			25.7	21.3
2	15.3	2.6	1.7	0.6					20.2	3.78
3	1.3	0.5							1.8	0.18
				OD + CH_3SCH_3						
0	6.2[a]	1.9[a]	6.2	1.9	3.2	2.2	2.5	1.0	25.0	81.8
1	23.7	3.4	10.7	7.7	2.6				48.0	16.8
2	20.2	3.5	3.3						27.0	1.4
				OH + CH_3SD						
0	16.1[a]	13.4[a]	16.1	13.4	4.1	2.9	3.2	2.1	71.3	74.8
1	5.0	3.5	4.6	3.8	1.3	4.4	3.9		26.5	21.3
2	0.5	0.9	0.7						2.1	3.8

[a] Populations in the dark (000) and (010) states were assumed to be equal to populations in the (020)/(100) and (030)/(110) states, respectively; P_3^0 is the statistical distribution. [b] The distribution from OD + CH_3SCH_3 was taken from ref 7.

$\nu_3 = 0$. The $\nu_3 = 1$ and $\nu_3 = 2$ wings are clearly distinguished, and the distribution for O−H stretching is $P_3(0:1:2:3) = 52:26:20:2$. The full distribution for HOD is presented in Table 2. This distribution differs somewhat from the first report,[7] because the spectrum obtained with the filter provided a more accurate measurement of the $\nu_3 = 0$ contribution. The improved HOD distribution has a lower $\nu_3 = 0$ population, but the nature of the P_3 distribution was not changed. The inverted H_2O and HOD distributions from OH(OD) + DMS reactions that were reported in ref 7 are included in Tables 1 and 2 for convenient reference.

The spectrum from the OH + CH_3SD reaction consists of overlapped H_2O and HOD emission in the 3200−3900 cm^{-1} range and the $\Delta\nu_1 = -1$ and $\Delta\nu_2 = -2$ HOD emission from $\nu_3 = 0$ states in the 2400−2900 cm^{-1} range; see Figures 1c and 2. The 2400−2900 cm^{-1} emission for OH + CH_3SD is stronger than that for the OD + CH_3SH reaction. For reaction 2, the O−H stretching is an "active" vibration connected with the reaction coordinate, whereas the ν_3 mode (O−H stretching) from reaction 4 represents the "passive" or "spectator" mode. The strongly overlapped HOD and H_2O emissions from the OH + CH_3SD reaction were separated in the following way. First, the H_2O spectrum from the OH + CH_3SCH_3 reaction that was measured in ref 7 was normalized to match a group of peaks that are specifically for the R-branch of H_2O in the 2800−3900 cm^{-1} region of the experimental spectrum. The H_2O spectra from reactions 1 and 3 look rather similar, and the H_2O contribution from (4b) and the possible contribution from reaction 1 due to the isotopic impurity in the CH_3SH sample was represented by one spectrum. Modeling of the HOD spectrum was done in the normal manner, after which a new adjustment of the H_2O contribution was made followed by the final fitting for the HOD spectrum. Five independently obtained spectra from the OH + CH_3SD reaction was fitted, and the fractional contribution of the H_2O emission varied by only ±10%. The vibrational distribution of HOD is given in Table 2 with the $P(\nu_3 = 0)$ fraction obtained from simulation of the 2400−2900 cm^{-1} experimental spectrum shown in Figure 2b. As expected, a decreasing distribution was found for the "passive" O−H vibration, $P_3(0:1:2) = 71 \pm 6:27:2$, with the majority of molecules (about 70%) in the ground $\nu_3 = 0$ state. The uncertainty is taken as the half of the population in the dark, ground vibrational state from the calculated statistical distribution. The population is close to the statistical distribution,

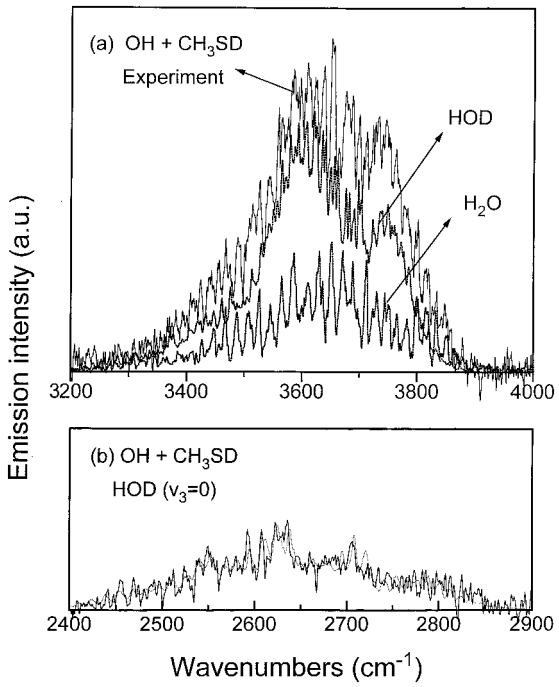

Figure 2. Comparison of experimental and calculated spectra from the OH + CH_3SD reaction. (a) The calculated $\Delta\nu_3 = -1$ spectra of HOD and the H_2O spectrum (from OH + DMS) are compared to the experimental spectrum (top) that has been corrected for the wavelength response. (b) Comparison of the experimental and calculated HOD spectra ($\Delta\nu_1 = -1$ and $\Delta\nu_2 = -2$) in the 2000−2900 cm^{-1} range.

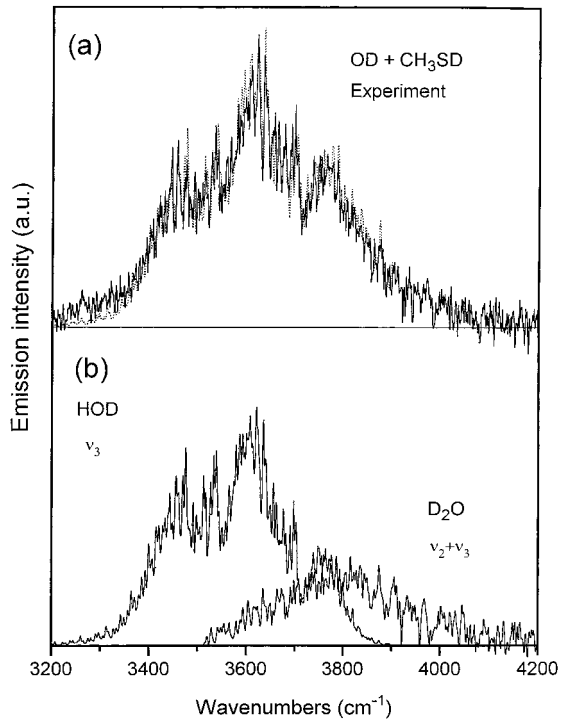

Figure 3. Comparison of experimental and simulated chemiluminescent spectra in the 3300−4200 cm^{-1} range produced in the reaction of OD with CH_3SD. (a) Experimental spectrum corrected for the detector response function (solid line) and the sum of the HOD and D_2O components (dotted spectrum). (b) Separated HOD emission from $\nu_3 = 1$ and 2 levels and the D_2O combination band from $\nu_2 + \nu_3$.

$P_3(0{:}1{:}2) = 75{:}21{:}4$, and the similarity to the HOD distribution from the unimolecular decomposition of CH_2DCH_2OH should be noted.[14]

The chemiluminescence from the OD + CH_3SD reaction shown in Figure 1d most clearly demonstrates the occurrence of channel 5b via the observation of HOD emission in the 3200−3900 cm^{-1} range along with the D_2O emission in the 2400−2900 cm^{-1} range. The spectrum from reaction 4 extends up to 4200 cm^{-1}, which is explained by the combination $\nu_2 + \nu_3$ emission from D_2O, originating from the 011−000 band[11] centered at 3965 cm^{-1}. The procedure for the separation of HOD and D_2O emission in the 3200−4200 cm^{-1} range is illustrated in Figure 3. It was assumed that the HOD spectrum from the OD + CH_3SD reaction was identical to that from the OD + CH_3SCH_3 reaction;[7] the vibrational distribution is presented in Table 2. The justification for this assumption is provided by the similar C−H bond energies in methanethiol and dimethyl sulfide, 92.4 ± 2.0 and 92.0 ± 1.4 kcal mol^{-1}, respectively.[15] The HOD spectrum from the DMS reaction in the 3200−3900 cm^{-1} range[7] was normalized to match the least noisy spectrum from reaction 5 in the 3200−3500 cm^{-1} region (Figure 3a) and then subtracted from the latter. The resulting spectrum, assigned to the combination $\nu_2 + \nu_3$ emission from D_2O is shown in Figure 3b. The 011 band[11] from this manifold is centered at 3965 cm^{-1}; the higher members (e.g., 022−011) extend to as low as 3500 cm^{-1}, covering a range of ∼500 cm^{-1}, which approximately equals the length of the ν_3 spectrum of D_2O. The experimental intensity was ∼0.6 of the D_2O intensity in 2400−2900 cm^{-1} range, which is similar to the ratios, 0.50 and 0.59, obtained for the ν_3 and $\nu_2 + \nu_3$ intensity ratio of H_2O from the OH + GeH_4 and HI reactions, respectively,[10] thus confirming the correctness of the separation of the HOD and D_2O bands that are shown in Figure 3b. Next, the HOD emission in five recorded spectra was determined as a difference between the total and the D_2O $\nu_2 + \nu_3$ emission (see Figure 3b). The average relative population in the $\nu_3 = 1$ and $\nu_3 = 2$ states, $P_3(1)/P_3(2) \approx 2$, was quite similar to that measured in OD + CH_3SCH_3 reaction. Therefore, we took the distribution for HOD from (5b) to be similar to that from the DMS reaction, $P_3(0{:}1{:}2) = 25{:}48{:}27$ (see Table 2). The simulated HOD spectrum with the added D_2O contribution is also shown in Figure 3a by the virtually identical superimposed dotted spectrum.

The D_2O distribution from reaction 5a was obtained by simulation of the D_2O spectrum shown in Figure 4. The experimental spectrum, corrected for the response function, is shown in Figure 4a, and the calculated 001 and 100 emission bands are shown in Figure 4c. The calculated spectrum presented in Figure 4b is for the D_2O distribution given in Table 1; the stretching distribution is $P_{1,3}(1{:}2{:}3) = 65{:}32{:}3$. Although the distribution is similar to the H_2O distribution from reaction 1, the H_2O distribution extends to the thermodynamic limit, whereas the thermochemically allowed 004−003 band of D_2O was not observed (see the statistical distribution in Table 1). The most probable explanation is that the vibrational populations of D_2O are more affected by collisional relaxation because of the smaller energy defects between sets of levels. The energy diagram in Figure 5, which includes all the D_2O vibrational levels allowed by the reaction exothermicity, shows that in addition to the close $\nu_{1,3}$ levels, a near coincidence exists between $3,\nu_2,0$ and $0,\nu_2+2$, 2 levels, which also are very close to $0,\nu_2+7,0$ level, and the $0,\nu_2,3$ level is close to $1,\nu_2+5,0$ level. Those levels with small energy defects could relax rapidly, and they are connected by dotted lines in Figure 5. The transfer of vibrational energy in cascade processes can explain why no emission was observed from the energetically available $\nu_{1,3} = 4$ level, and only very weak emission was observed from $\nu_{1,3} = 3$. Instead, we see an apparent overpopulation of $\nu_{1,3} = 2$, $\nu_2 = 2$ and 4. The observed overpopulation of the $\nu_{1,3} = 1$, $\nu_2 = 4$ and 5 states is less easy to understand, because the $2,\nu_2,0$

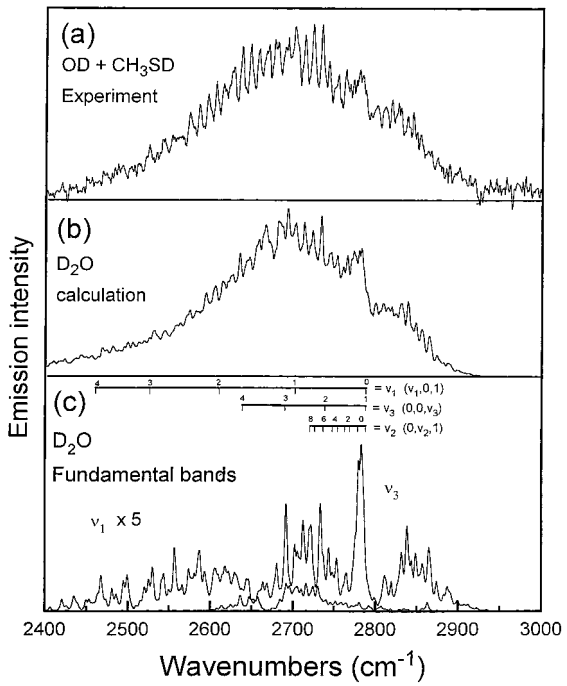

Figure 4. Comparison of the D_2O chemiluminescent and calculated spectra produced in the reaction of OD with CH_3SD: (a) experimental spectrum corrected for the detector response function; (b) calculated spectrum; (c) 100 and 001 fundamental emission bands, the band centers for spectra corresponding to several bending and stretching levels are indicated.

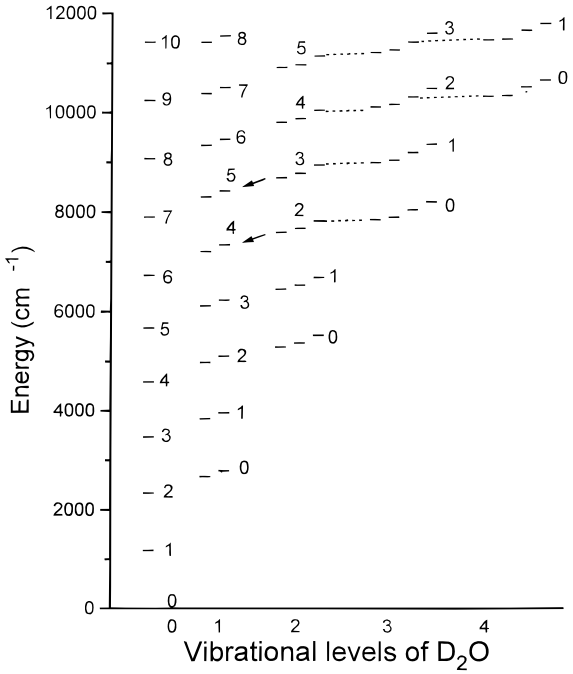

Figure 5. Vibrational energy levels of the D_2O molecule. The energies were taken from spectroscopic measurements[12] and theoretical work.[13] The energy for levels with $\nu_2 > 4$ were evaluated by extrapolation. The ordinate denotes values for either ν_1 or ν_3.

and $0,\nu_2+2,1$ levels are somewhat more distant (see the arrows in Figure 5). However, the accuracy of the energy levels with $\nu_2 \geq 4$ is not very high, and some energy exchange may take place between the $2,\nu_2,0$ and $0,\nu_2+2,1$ levels during collisions. The energy diagram suggests that levels below 7000 cm^{-1} should not be affected by relaxation processes, while higher states may be more strongly affected. The levels with $\nu_3 = 0$, $\nu_2 < 6$ are well separated from other levels, and the measured $P_{1,3}(0)$ is not expected to be higher than the nascent value. The nascent $P_{1,3}(0)$ population is expected to be somewhat less than statistical, which sets an upper limit to $P_{1,3}(0)$ of 36%. Since relaxation changes the relative $P_{1,3}(\nu_{1,2}\neq 0)$ populations, we decided to estimate $P_{1,3}(0)$ for D_2O by analogy to the H_2O distribution from reaction 1 with comparison to the statistical distribution rather than from the surprisal plot. The vibrational distribution obtained previously[7] for H_2O from OH + CH_3SH is $P_{1,3}(0,1,2,3) = 45, 39, 16, 2$. The $P_{1,3}(0)$ value was determined from the linear surprisal plot. This distribution is similar to the statistical H_2O distribution calculated for $E_{av} = 34.4$ kcal mol^{-1}, but $P_{1,3}(0)$ is a factor of 0.85 lower than the statistical value. Higher vibrational levels can be excited in D_2O for the same available energy, and the statistical distribution is $P_{1,3}{}^0(0,1,2,3,4) = 36, 34, 21, 7, 1$. From analogy to the H_2O case, we multiplied $P_{1,3}{}^0(0)$ by 0.85 to obtain $P_{1,3}(0) = 30$. The full renormalized D_2O distribution from reaction 5a becomes $P_{1,3}(0,1,2,3) = 30 \pm 6, 43, 25, 2.5$; the upper limit for $P_{1,3}(0) = 36$ is the statistical value.

3.2. Branching Fraction for the Reaction of OD with CH_3SD. To determine the product branching fraction for OD + CH_3SD, the relative D_2O and HOD emission intensities were measured (as areas) from the CH_3SD and $(CH_3S)_2$ systems in the 2400−2900 cm^{-1} and 3200−4200 cm^{-1} ranges, respectively, with correction for the detector response function. In these measurements, the HOD emission from $\nu_3 = 0$ states in the 2400−2900 cm^{-1} range (see Figure 1b) was neglected and the 2400−2900 cm^{-1} intensity from CH_3SD was totally assigned to the $\Delta\nu_{1,3} = -1$ transitions of D_2O. The HOD intensity in seven recorded spectra was obtained as a difference between the total intensity and the intensity of the D_2O $\nu_2 + \nu_3$ emission, and the average ratio is $I_{HOD}/I_{D_2O} = 1.12 \pm 0.22$.

The experimental intensity ratio can be converted to the ratio of HOD to D_2O concentrations using the expression

$$\frac{[\mathrm{HOD}]}{[\mathrm{D_2O}]} = \frac{I_{\mathrm{HOD}}\beta_{\mathrm{D_2O}}S_v(\nu_3,\mathrm{D_2O})}{I_{\mathrm{D_2O}}\beta_{\mathrm{HOD}}\,S_v(\nu_3,\mathrm{HOD})} \qquad (6)$$

where $S_v(\nu_3)$ are the ν_3 fundamental band sum intensities, and the coefficients $\beta = \beta(P_3(\nu_3))$ give the fraction of the ν_3 populations that is in the emitting levels which can be observed. The β factors depend on the given vibrational distribution. These coefficients can be expressed as $\beta = \sum_i \alpha_i P_3(\nu_i)$, where the band strength coefficients α_i for the equilibrated emission bands ($\nu_1/\nu_2/\nu_3$) are defined as $S_v(\nu_1/\nu_2/\nu_3) = \alpha_i S_v(001)$ and their numerical values[10] for H_2O ($i = \nu_{1,3} = \nu_1 + \nu_3$) are $\alpha_1 = 0.43$, $\alpha_2 = 0.72$, and $\alpha_3 = 0.91$ for HOD ($i = \nu_3$) are $\alpha_1 = 1.0$, $\alpha_2 = 1.8$, and $\alpha_3 = 2.3$, respectively. The band strength coefficients for D_2O equilibrated ($\nu_{1,3},\nu_2$) bands are $\alpha_1 = 0.45$, $\alpha_2 = 0.82$, and $\alpha_3 = 1.11$ (see Appendix). The efficiency coefficients are $\beta_{D_2O} = 0.41 \pm 0.03$ and $\beta_{HOD} = 0.90 \pm 0.05$, and the ratio of the fundamental band sum intensities is $S_v(\nu_3,D_2O)/S_v(\nu_3,HOD) = 1.00/4.47$, as determined in Appendix. Substituting the numerical values in eq 6, we have $[HOD]/[D_2O] = 0.13 \pm 0.02$ and a branching fraction of 0.11 ± 0.02. The statistical uncertainty of ± 0.02 from the seven spectra was doubled to recognize approximations inherent in spectral deconvolution and the β-factors.

Comparison of the spectra from OD + DMDS and OD + CH_3SD systems in the 3200−4200 cm^{-1} range permitted an estimate of the isotopic impurity of the CH_3SD sample. Five measured spectra from OD + CH_3SD were averaged and compared to the spectra from OD + DMDS system and to the HOD spectrum from OD + CH_3SH reaction. The best fit to

the OD + CH_3DS spectrum was achieved when the intensity of the HOD spectrum added to the DMDS spectrum was less than 0.10 of the total intensity. Taking into account that D_2O-($\nu_2+\nu_3$) emission constitutes about 30% of the total intensity, the maximum value of 0.14 was obtained for the ratio of HOD emission intensities from OD + CH_3SH and OD + CH_3SD reactions. Since HOD formation is only ~0.11 of the total rate of the OD + CH_3SD reaction and since the emission efficiencies are $\beta_{HOD}(CH_3SH) = 0.60 \pm 0.06$ and $\beta_{HOD}(DMS) = 0.90 \pm 0.05$, the maximum contribution from CH_3SH can be estimated as $0.14 \times 0.11 \times (0.95/0.54) = 0.03$, or 3%, which is in accord with the stated isotopic purity, and we can conclude that the H/D exchange in the CH_3SD sample during transport through the lines was not important.

3.3. Branching Fraction for the Reaction of OH with CH_3SD. The HOD emission intensity was obtained from five experiments as the difference between the total integrated intensity in the 3200−4000 cm^{-1} range and the intensity of the H_2O contribution. The average $I_{H_2O}/I_{HOD} = 0.40 \pm 0.04$ ratio was obtained; the error limits correspond to the standard deviation for the five spectra. This ratio is somewhat uncertain because of the difficulty of deconvolution of the H_2O and HOD components; see Figure 2. The H_2O intensity includes the H_2O product from the OH + CH_3SH reaction due to the 3% isotopic impurity. Assuming that both H_2O spectra are similar to that from the OH + DMS reaction, the ratio of H_2O to HOD concentrations can be determined from eq 7.

$$\frac{[H_2O]}{[HOD]} = \frac{I_{H_2O}\beta_{HOD}S_\nu(\nu_3,HOD)}{I_{HOD}\beta_{H_2O}S_\nu(\nu_3,H_2O)} \qquad (7)$$

With $\beta_{HOD} = 0.27 \pm 0.05$, $\beta_{H_2O} = 0.38 \pm 0.03$, and $S_\nu(\nu_3,HOD)/S_\nu(\nu_3,H_2O) = 1.3$, we obtained $[H_2O]/[HOD] = 0.37$. Adjustment for the isotopic impurity (3%) reduces this ratio significantly, and the branching fraction for reaction 4 is 0.24 ± 0.08, which is 2 times larger than the branching ratio for reaction 5. Although the value has considerable experimental uncertainty, in part because of the small CH_3SH impurity, the larger fraction for abstraction for reaction 4 implies that a large inverse secondary kinetic-isotope effect exists for reactions 4a and 5a. This isotope effect arises from the altered rate constant for decomposition of the adduct, which presumably is in competition with redissociation. Additional support for this idea is provided below by comparing the total rate constant ratio for OH and OD + CH_3SH.

Since practically equal rate coefficients, $(3.24 \pm 0.19) \times 10^{-11}$ and $(3.17 \pm 0.15) \times 10^{-11}$ molecules cm^{-3} s^{-1}, were found[4] for the OH + CH_3SD and OH + CH_3SH reactions, a product branching fraction of ~0.24 can be predicted for the C−H abstraction channel of the OH + CH_3SH reaction. If this prediction is correct, the primary isotope effect for elimination of H_2O from $CH_3S(OH)H$ vs HOD from $CH_3S(OH)D$ must be small. Presumably, the branching fraction for OD + CH_3SH will resemble that for reaction 5.

3.4. Kinetic Isotope Effects. First, consider the small KIE observed by Hynes and Wine[3] for the reaction of OH with CD_3SH and CH_3SH. They obtained $k(OH+CH_3SH) = 3.24 \times 10^{-11}$ and $k(OH+CD_3SH) = 2.76 \times 10^{-11}$ molecules cm^{-3} s^{-1}, which gives $k_H/k_D = 1.17$. A primary KIE of $k_H/k_D = 2.27$ was found[16] for the OH + CH_3SCH_3 ($k = 4.40 \times 10^{-12}$ cm^{-3} s^{-1}) vs the CD_3SCD_3 ($k = 1.94 \times 10^{-12}$ cm^{-3} s^{-1}) reactions. If we assume that the primary KIE for channel 1b is similar to this value and that this channel is 0.24 of the total reaction rate, the overall KIE for OH + CD_3SH and CH_3SH can be calculated as $k_H/k_D = 1.00/(0.24/2.27)+0.76 = 1.00/0.87 = 1.15$ in agreement with the result of Wine et al.

A measurable secondary KIE ($k_{OH}/k_{OD} \approx 0.7$) for reactions 1 and 2 has been already reported in our previous work[7] from comparison of the individual intensities from these reactions with that of the DMS reactions. In that work, we used the value of the inverse secondary KIE for OH/OD reactions with CH_3SCH_3, $k_{OH}/k_{OD} = 0.85$, measured by Stickel.[17] In the present work, we made direct comparisons of the H_2O and HOD intensities from reactions 1 and 2 for the same conditions and approximately equal concentrations of CH_3SH and OH and OD. The KIE was obtained from the intensity ratio as

$$\frac{k_{OH}}{k_{OD}} = \frac{I_{H_2O}\beta_{HOD}S_\nu(\nu_3,HOD)}{I_{HOD}\beta_{H_2O}S_\nu(\nu_3,H_2O)} = 0.67 \pm 0.10 \qquad (8)$$

which confirmed the previous estimate.[7] This value corresponds to the overall kinetic-isotope effect for channels a plus b. By comparison of the relative emission intensities from reactions 4 and 5, the specific KIE for channels a and b can be obtained. The method is quite similar to that which was used to determine branching ratios, except that adjustment for the different reagent concentrations must be made. Thus, to obtain the relative rate of (4a) to (5a), we compared the HOD and D_2O emission intensities from the OH + CH_3SD and OD + CH_3SD reactions, respectively:

$$\frac{k_{OH}}{k_{OD}} = \frac{I_{HOD}[CH_3SD][OD]\beta_{D_2O}S_\nu(\nu_3,D_2O)}{I_{D_2O}[CH_3SD][OH]\beta_{HOD}S_\nu(\nu_3,HOD)} = 0.60 \pm 0.05 \qquad (9)$$

that is, the OD reaction is nearly 2 times faster than the OH reaction.

In addition to the aforementioned reaction with DMS,[17] faster OD reactions at 298 K have been found for several other hydroxyl reactions; the KIE are CH_4[18] (0.91 ± 0.04), n-C_4H_{10}[19] (0.87 ± 0.14), DCl[21] (0.85 ± 0.15), and H_2O[22] (0.74 ± 0.20). All these reactions have small activation energy barriers and they are supposed to proceed by direct abstraction (except possibly the OH + H_2O reaction).[22] For a bimolecular reaction, the transition state theory (TST) rate constant takes the form

$$k = \frac{kT}{h}\frac{F^\ddagger}{F_{OH}F_Y}\exp\left(-\frac{\Delta E^\ddagger_0}{kT}\right) \quad \Delta E^\ddagger_0 = E^\ddagger_0 + E^\ddagger_z - E_z^{OH+Y} \qquad (10)$$

where F_{OH} and F_Y are the partition functions of the OH(OD) radical and reagent molecule and $F^\ddagger$ is the partition function for the TS. The threshold energy, $\Delta E_0^\ddagger$, is given by the electronic energy plus the difference in zero-point energies of transition state and reagents. Detailed analysis of the secondary KIE for OH(OD) + CH_4 was made[18] using the ab initio TS parameters.[23] In this case, the contributions from rotational/translational, vibrational and zero-point energy (ZPE) factors were equal to 1.74, 0.79, and 0.78, respectively, giving a total KIE of 0.89. The main factor giving an inverse KIE is the change in ZPE due to the four new vibrations in the tight transition state. This is a general property of OH/OD direct abstraction reactions because of the development of the bending mode in the transition state, which affects the zero-point energy.[24,25] The vibrational factor is determined by the low frequencies in the TS, since the other vibrational frequencies give $F_i = 1.0$ at 300

TABLE 3: Vibrational Frequencies (cm^{-1}) of $CH_3S(OH)H$ and $CH_3S(OD)H$ Adducts and Transition States Used to Estimate the Secondary Kinetic Isotope Effect

	adduct[a]		TS[b]		TS[c]		molecule	
mode	(OH)	(OD)	(OH)	(OD)	(OH)	(OD)	OH	OD
OH stretch	3590	2614	3590	2614	3240	2689	3653	2658
O−H bend	816	617	1387	1008	1490	1028		
			332	256				
S−O stretch	465	450	563	478				
O−H′ stretch			784	746	827	744		
OH torsion	289	242						
S−OH bend	239	256			223[d]	156[d]		
S−OH bend	44	40						
I (IR)[e] (amu Å^2)					0.80	1.19		

[a] The frequencies of the OH adduct are from ref 28a with a scaling factor of 0.98. The OD adduct frequencies were obtained in the same way from 28b. [b] Three-centered $CH_3S(OH)H'$ or $CH_3S(OD)H'$ transition state. [c] Linear transition state for the direct abstraction reaction (ref 18). [d] H′−OH bend. [e] The moment of inertia for the internal rotation of hydroxyl.

K. Taking into account the large number of recent high-level theoretical studies,[23,24,26] the H−O−H′−X transition state for the direct abstraction can be characterized as tight with ∠OH′X ≈ 160° (nearly collinear atom transfer), R(X−H′) ≈ 1.2 Å, and R(O−H′) ≈ 1.3 Å. The frequencies for such a "linear" TS can be regarded as rather generic, and the values in Table 3 from ref 18 can be considered as representative. The lowest frequency mode of these TSs is usually treated as a hindered rotation, and some difference exists in its description because the internal rotation can be considered either as a rotation of hydroxyl around the XH′O axis,[26b,c] or as a rotation of X around the reactive C−H′ bond.[26a] The moment of inertia for the internal rotation in Table 3 refers to the former method of description. The ZPE contribution to the rate constant ratio at room temperature is usually about 0.5, as shown in the theoretical study[24] of the OH/OD reactions with NH_3 using variational TST with semiclassical tunneling and ab initio calculation of the TS geometries and frequencies at the QCIT/PTZ+ level of theory. The calculated rotational and vibrational factors were 1.54 and 0.92 and tunneling and variational corrections gave a factor of 1.24, resulting in the inverse KIE of $k_{OH}/k_{OD} = 0.93$. For abstraction reactions with lower activation energies, the ZPE contribution decreases and, in general, the balance between the rotational and ZPE contributions can give small inverse or a normal secondary KIE, which is not expected to differ much from unity.

We decided to apply TST to reactions 1 and 2 to see if the KIE for channel b agrees with the assumption of formation of the $CH_3S(OH)H$ adduct, which subsequently dissociates in the rate-limiting step to yield water and CH_3S through a three-centered transition state involving a sulfur bonded H atom. This assumption is based on the experimental facts that elimination of H_2O from the DMS·OH adduct with a binding energy of 11 ± 3 kcal mol^{-1} has been never observed,[27] plus the abstraction-like vibrational distributions (Tables 1 and 2) of reaction 3. The ab initio study of the OH + CH_3SH adduct by Wilson and Hirst[6] found that $\Delta H° = -2.5$ kcal mol^{-1} for the $CH_3S(OH)H$ adduct. In the theoretical study of the OH + DMS system,[27] McKee notes that the DMS·OH adduct is a "difficult case" for ab initio treatment due to the nearly equal spin density on OH and sulfur resulting in a strong mixing of the OH and DMS molecular orbitals. That is why even the high QCISD-(T)/6-31+G(2d,p) level of calculations gives, at least, a 4 kcal mol^{-1} underestimate for the OH binding to DMS. Since the calculations for $CH_3S(OH)H$ were made at the same level of theory, the binding energy of the $CH_3S(OH)H$ adduct may be ~5 kcal mol^{-1}. When adducts are part of the mechanism, the experimental E_a value need not be a measure of any particular barrier height and, in fact, they often are negative. Fortunately, to examine the kinetic-isotope effects the absolute threshold energy of the TS is not required. We estimated the essential vibrational frequencies of the $CH_3(OH)SH$ and $CH_3S(OD)H$ adducts, and the frequencies that are influenced most by the isotopic substitution are presented in Table 3. These frequencies were obtained by scaling (0.98) the frequencies values for the DMS·OH[28a] and DMS·OD[28b] adducts calculated at the MP2/6-31G(2d) level. The geometry of DMS·OH corresponds to a very long S−O bond (2.05 Å) that is perpendicular to the CSC plane; the R(S−O) was 1.91 Å for the $CH_3S(OH)H$ adduct.[6] Our calculation[28b] reproduced the structure and frequencies for DMS·OH reported by McKee, and the frequencies selected for the $CH_3S(OH)H$ and $CH_3S(OD)H$ adducts (see Table 3) should be reasonable estimates. The frequencies of the OH or OD vibrations in the TS (stretching and in-plane and out-plane bendings) were assumed to be equal to the corresponding TS frequencies for the four-centered unimolecular decomposition reactions $CH_2DCH_2OH \rightarrow H_2O$ and $CH_2DCH_2OD \rightarrow HOD$ that were obtained by ab initio calculation at the MP2(FULL)/6-311G(d) level.[14] The frequencies of the S−O−H′ three-membered ring are less sensitive to the OD for OH substitution, and we choose two, which could most reliably represent the S−O and O−H′ stretchings. Although the latter choice is rather arbitrary, it has no significant impact on KIE unless very low frequencies are involved; see Table 3. Neglecting tunneling and recrossing effects, the unimolecular TST rate constant can be presented as

$$k = \frac{kT}{h}\frac{F^{\ddagger}}{F_A}\exp\left(-\frac{\Delta E^{\ddagger}_0}{kT}\right)\Delta E^{\ddagger}_0 = \mathrm{E}^{\ddagger}_0 + \mathrm{E}^{\ddagger}_z - \mathrm{E}^{\mathrm{A}}_z \quad (11)$$

where $F^{\ddagger}$ and F_A are the partition functions for the TS and the adduct, and E^{A}_z and $E^{\ddagger}_z$ are the zero-point vibration energies of the adduct and TS, respectively, and $E^{\ddagger}_0$ is the potential energy barrier. The ratio of rate constants for our case is given in (12), where the prime and double prime represent H and D labels, respectively.

$$\frac{k'}{k''} = \frac{\left(\frac{I^{\ddagger\prime}}{I^{\ddagger\prime\prime}}\right)^{1/2}\prod_{k=1}^{s-1}\frac{[1-\exp(-h\nu_k{}^{\ddagger\prime\prime}/kT)]}{[1-\exp(-h\nu_k{}^{\ddagger\prime}/kT)]}\exp(-E^{\ddagger}{}_z'/kT + E^{\ddagger}{}_z''/kT)}{\left(\frac{I''}{I'}\right)^{1/2}\prod_{k=1}^{s}\frac{[1-\exp(-h\nu_k{}^{\ddagger\prime\prime}/kT)]}{[1-\exp(-h\nu_k'/kT)]}\exp(-E^{\mathrm{A}\prime}{}_z/kT + E^{\mathrm{A}\prime\prime}{}_z/kT)} \quad (12)$$

The translational partition functions exactly cancel, the moment of inertia ratio is essentially unity, and the vibrational partition function ratio will include only these vibrations given in Table 3. The temperature for the calculation was 300 K. This situation is nearly a classic example for an inverse secondary isotope effect, because the system changes from a very loose reactant state to a tight transition state with development of more zero-point energy in the TS. If the moment of inertia factor is taken as unity, the isotope effect is (0.96)(0.47) = 0.45. Our ZPE factor of 0.47 is just an estimate, but surely this estimate is illustrative that an inverse KIE would be expected and that the experimental value is reasonable. The estimate also suggests that the inverse kinetic-isotope effects for processes giving water as a product may be generally larger for those that proceed by addition−elimination rather than by direct abstraction.

In this discussion, we used canonical transition-state theory to describe the elimination rate constants and we have ignored the OH + CH_3SH addition step. Canonical theory may not apply if the lifetimes of the adducts are short. On the other hand, the binding energies of the adducts are far too small to justify using RRKM models to describe the unimolecular step. In this context, the large inverse isotope effect (factor of 3) reported for Cl + C_2H_4 is relevant.[29] The reduced unimolecular dissociation rate constant for $ClCD_2CD_2$ vs $ClCH_2CH_2$ radicals enhanced the net bimolecular rate for removal of Cl atoms by C_2D_4. A complete description of the secondary isotope effect for the OD reaction in (1a) and (5a) may require consideration of the addition and redissociation steps, as well as the elimination step.

Finally, some comment about the apparently small primary KIE for elimination of HOD from $CH_3S(OH)D$ vs $CH_3S(OH)H$ is needed. The zero-point energy changes expected for the migrating H(D) atom from the −S−H(−S−D) moiety is balanced by the bending mode frequency associated with the H_2O(HOD) moiety of the transition state. Thus, the net zero-point energy difference is small.

Conclusions

The infrared emission spectra from the OH(OD) plus CH_3-SD reactions has confirmed the claim[2] that the majority of the reaction occurs from the sulfur end of the molecule to give either HOD (or D_2O). Simulation of the spectra from these reactions and new spectra from the OH(OD) + CH_3SH reactions are in agreement with the stretch and bend vibrational distributions of the water product molecules assigned previously.[7] On the basis of the much larger rate constant for CH_3SH vs CH_3SCH_3, the primary kinetic-isotope effects, and the H_2O and HOD vibrational distributions, the mechanism for OH(OD) + CH_3-SD is verified to be addition to give an $CH_3S(OH)D$ or CH_3S-(OD)D adduct, which subsequently redissociates or eliminates HOD(D_2O). Detailed analysis of the emission spectra shows that the branching fraction for addition−elimination channel is 0.89 and 0.76 for the OD + CH_3SD and OH + CH_3SD reactions, respectively. The remainder corresponds to direct abstraction from the methyl end of the molecule. The enhancement of the direct abstraction pathway for the OH reaction is associated with an inverse secondary kinetic-isotope effect for the elimination step from the $CH_3S(OH)D$ and $CH_3S(OD)D$ adducts. Such an inverse effect was demonstrated by directly comparing the H_2O and HOD intensities from OH + CH_3SH and OD + CH_3SH, which gave $k_{OH}/k_{OD} = 0.67 \pm 0.10$ for the overall kinetic isotope effect. The abstraction components were removed to obtain 0.6 ± 0.1 as the inverse effect for addition−elimination.

On the basis of the similarity in rate constants for OH + CH_3SH vs CH_3SD, and the expected small primary kinetic-isotope effect for elimination of H_2O or HOD, we predict that the branching fractions for OH + CH_3SH will be approximately 0.24 for abstraction and 0.76 for addition−elimination. We, thus, recommend these branching fractions when considering secondary reactions of CH_3S and CH_2SH radicals in the oxidation of CH_3SH.

Appendix: Calculation of 100 and 001 Emission Bands for D_2O

In the present work, the 443 most intense lines of the ν_3 band and 424 lines of the ν_1 band were selected from the list of Papineau et al.[30] The absorption vibration−rotation intensity of a line was calculated according to the expression

$$I_{abs} = \frac{8\pi\nu}{3hc}\frac{g}{Q(T)}\exp(-E_r/kT)\,|^{\nu}\mu|^2 \qquad (1A)$$

where ν is the transition frequency, g is the degeneracy due to nuclear spin of the lower level, $Q(T)$ is the rotational partition function, $E_r = E_r(J,K_a,K_c)$ is the energy of the lower level and $^{\nu}\mu = {}^{\nu}\mu(J,K_a,K_c)$ is the vibration−rotation dipole moment matrix element of the transition. The latter was calculated using the expansion of the transformed dipole moment developed to determine the H_2O fundamentals.[31] In this method, a dipole moment operator for a given vibration−rotation transition is presented as $^{\nu}\mu = \sum_i {}^{\nu}\mu_j {}^{\nu}A_j$, where $^{\nu}\mu_j$ are numerical constants and $^{\nu}A_j$ are the matrix elements.[31] The expansions have the form $^1\mu = {}^1\mu_1{}^1A_1 + {}^1\mu_4{}^1A_4 + {}^1\mu_5{}^1A_5$ for the 100 and $^3\mu = {}^3\mu_1{}^3A_1 + {}^3\mu_4{}^3A_4 + {}^3\mu_6{}^3A_6$ for the 001 bands. $^1A_1$ is just the cosine matrix element, and the first-order constants $^1\mu_1$ and $^3\mu_1$ are the average values of the dipole derivatives with respect to the corresponding normal coordinate. The latter were measured,[32] giving for D_2O $^1\mu_1 = -0.017$ and $^3\mu_1 = 0.0614$. Numerical constants $^{\nu}\mu_j$ (ν = 1 and 3) were calculated on the basis of the D_2O spectroscopic constants using general expressions[33] to give the following values: $^1\mu_4 = 0.000906$ D, $^1\mu_5 = -0.00270$ D, $^3\mu_4 = -0.000811$ D, and $^3\mu_6 = 0.000303$ D. In the calculation of intensities, the interactions between 48 close rotational levels of 100 and 001 states were taken into account. The main effect of these interactions, for which states with $J > 7$ and $K = 6-8$ are involved, is borrowing intensity for 100 transitions in accordance with the mixing coefficients.[30] The sum intensities of the calculated absorption bands are $S_\nu(001,D_2O) = 3.85 \times 10^{-18}$ and $S_\nu(100,D_2O) = 3.85 \times 10^{-18}$ cm^{-1}/molecules cm^{-2}. The relative *emission* intensities were obtained according to the general relation between the Einstein transition probabilities of absorption and spontaneous emission. A conversion expression may be written as

$$I_{em} = (\text{const})I_{abs}\nu^3(g_h/g_l)\exp\{(\nu_0 - \nu)/kT\} \qquad (2A)$$

where ν_0 is the band center, subscripts h and l denote upper and lower levels. The statistical weights of the even and odd rotational states of D_2O are $g = 1$ and $g = 2$, respectively. The calculated emission fundamental bands are shown in the bottom of Figure 3.

To obtain the relation between the intensities of the H_2O and D_2O bands, a similar calculation was carried out for the H_2O 001 and 100 fundamentals of H_2O. The same method was applied to calculate the intensities of the 228 most intense lines of the ν_3 band and 204 lines of the ν_1 band with positions and assignments taken from the HITRAN database.[34] Actually, we repeated the calculation of Flaud and Camy-Peyret[31] for a restricted number of lines. The statistical weights of the even and odd rotational states for H_2O are $g = 3$ and $g = 1$,

respectively. The obtained sum intensities for the absorption bands are $S_v(001,H_2O) = 7.0 \times 10^{-18}$ and $S_v(100,H_2O) = 5.0 \times 10^{-18}$ cm^{-1}/molecules cm^{-2}. Comparison with the HITRAN sum intensity values, $S_v(001,H_2O) = 7.2 \times 10^{-18}$ and $S_v(100,H_2O) = 5.0 \times 10^{-18}$ cm^{-1}/molecules cm^{-2} shows that all the important transitions were taken into account. The partition functions are 174.6 (H_2O) and 337.7 (D_2O) at 298 K.

The ratio of 100 to 001 sum emission intensity for D_2O is $S_v(100,D_2O)/S_v(001,D_2O) = 0.134$ compared to the H_2O value of 0.089, indicating that accounting for the $\Delta\nu_1 = -1$ transitions is even more important for simulation of D_2O spectra than for H_2O spectra. Our calculations gave the following ratios for the emission band sum intensities of the isotopic water molecules: $S_v(001,H_2O)/S_v(001,D_2O) = 3.44$ and $S_v(001,HOD)/S_v(001,D_2O) = 4.47$. The latter ratio was obtained using the relation between the absorption sum band intensity values[34] for H_2O and HOD ($S_v(001,H_2O) = 7.2 \times 10^{-18}$ and $S_v(001,HOD) = 9.4 \times 10^{-18}$ cm^{-1}/molecules cm^{-2}.

The emission efficiency of the excited D_2O molecules after equilibration is estimated with the help of β coefficients, which show what part of the 001 band intensity is observed in the experiments. These coefficients can be expressed as $\beta = \sum_i \alpha_i P_3(\nu_i)$, where the band strength coefficients α_i for the equilibrated emission bands ($\nu_1/\nu_2/\nu_3$) are defined as $S_v(\nu_1/\nu_2/\nu_3) = \alpha_i S_v(001)$ with $i = \nu_{1,3} = \nu_1 + \nu_3$ in the case of H_2O and $i = \nu_3$ in the case of HOD. We determine α values for D_2O equilibrated ($\nu_{1,3},\nu_2$) bands according to the Boltzmann weight of their constituents, which are practically independent of ν_2:

$$(1,\nu_2) = 0.365(0,\nu_2,1) + 0.635(1,\nu_2,0),\ \nu_2 = 0-6;$$

$$(2,\nu_2) = 0.163(0,\nu_2,2) + 0.337(1,\nu_2,1) + 0.500(1,\nu_2,0),\ \nu_2 = 0-4;$$

$$(3,\nu_2) = 0.075(0,\nu_2,3) + 0.164(1,\nu_2,2) + 0.338(2,\nu_2,1) + 0.428(3,\nu_2,0),\ \nu_2 = 0-2.$$

Using the relation between the intensities of 001 and 100 emission bands of D_2O, $S_v(\nu_1) = 0.134 S_v(\nu_3)$, as calculated above, we obtain $\alpha_1 = 0.45$, $\alpha_2 = 0.82$, and $\alpha_3 = 1.11$. It means, for example, that in the case of 100% yield of D_2O in the $\nu_1 = 0$, $\nu_3 = 1$ state, only $0.45 S_v(\nu_3)$ of the intensity is observed because more than half of the molecules would be converted to the $\nu_1 = 1$, $\nu_3 = 0$ reservoir state.

Acknowledgment. The work at Kansas State University was supported by the U.S. National Science Foundation, Grant CHE-9505032. We thank Dr. Pedro Muiño, Kansas State University, for the ab initio calculations of the $CH_3S(OD)CH_3$ adduct (ref 28b).

References and Notes

(1) Tyndall, G. S.; Ravishankara, A. R. *Int. J. Chem. Kinet*. **1991**, *23*, 483.
(2) Tyndall, G. S.; Ravishankara, A. R. *J. Phys. Chem.* **1989**, *93*, 4707.
(3) Hynes, A. J.; Wine, P. H. *J. Phys. Chem.* **1987**, *91*, 3672.
(4) Wine, P. H.; Thompson, R. J.; Semmes, D. H. *Int. J. Chem. Kinet*. **1984**, *16*, 1623.
(5) Hatakeyama, S.; Akimoto, H. *J. Phys. Chem*. **1983**, *87*, 2387.
(6) (a) Wilson, C.; Hirst, D. M. *J. Chem. Soc., Faraday Trans*. **1995**, *91*, 3783. (b) Wilson, C.; Hirst, D. M. *Prog. React. Kinet.* **1996**, *21*, 69.
(7) Butkovskaya, N. I.; Setser, D. W. *J. Phys. Chem*. **1998**, *102*, 6395.
(8) Butkovskaya, N. I.; Setser, D. W. *Chem. Phys. Lett*., in press.
(9) Butkovskaya, N. I.; Setser, D. W. *J. Phys. Chem*. **1996**, *100*, 4853.
(10) Butkovskaya, N. I.; Setser, D. W. *J. Chem. Phys.* **1997**, *106*, 5028.
(11) Benedict, W. S.; Gailar, N.; Plyler, E. K. *J. Chem. Phys.* **1956**, *24*, 1139.
(12) (a) Bykov, A. D.; Lopasov, V. P.; Makushkin, Yu. S.; Sinitsa, L. N.; Ulenikov, O. N.; Zuev, V. E. *J. Mol. Spectrosc.* **1982**, *94*, 1. (b) Bykov, A. D.; Makarov, V. S.; Moskalenko, N. I.; Naumenko, O. V.; Ulenikov, O. N.; Zotov, O. V. *J. Mol. Spectrosc.* **1987**, *123*, 126. (c) Ormsby, P. S.; Rao, K. N.; Winnewisser, M.; Winnewisser, B. P.; Naumenko, O. V.; Bykov, A. D.; Sinitsa, L. N. *J. Mol. Spectrosc.* **1993**, *158*, 109. (d) Bykov, A. D.; Naumenko, O. V.; Sinitsa, L. N.; Winnewisser, B. P.; Winnewisser, M.; Ormsby, P. S.; Rao, K. N. *J. Mol. Spectrosc.* **1994**, *166*, 169.
(13) Halonen, L.; Carrington, T., Jr. *J. Chem. Phys.* **1988**, *88*, 4171.
(14) Butkovskaya, N. I.; Setser, D. W. *J. Chem. Phys.* **1996**, *105*, 8064.
(15) Berkowitz, J.; Ellison, G. B.; Gutman, D. *J. Phys. Chem*. **1994**, *98*, 2744.
(16) Hynes, A. J.; Wine, P. H.; Semmes, D. H. *J. Phys. Chem*. **1986**, *90*, 4148.
(17) Stickel, R. E.; Zhao, Z.; Wine, P. H. *Chem. Phys. Lett*. **1993**, *212*, 312.
(18) Gierczak, T.; Talukdar, R. K.; Herndon, S. C.; Vaghjiani, G. L.; Ravishankara, A. R. *J. Phys. Chem*. **1997**, *101*, 3125.
(19) Paraskevopoulos, G.; Nip, W. S. *Can. J. Chem*. **1980**, *58*, 2146.
(20) Smith, I. W. M.; Williams, M. D. *Ber. Bunsen-Ges. Phys. Chem*. **1985**, *89*, 319.
(21) Butkovskaya, N. I.; Setser, D. W. *J. Chem. Phys.* **1998**, *108*, 2434.
(22) Dubey, M. K.; Mohrschladt, R.; Donahue, N. M.; Anderson, J. G. *J. Phys. Chem*. **1997**, *101*, 1494.
(23) Truong, T. H.; Truhlar, D. G. *J. Chem. Phys*. **1990**, *93*, 1761.
(24) (a) Corchado, J. C.; Espinosa-Garcia, J.; Hu, W.-P.; Rossi, I.; Truhlar, D. G. *J. Phys. Chem*. **1995**, *99*, 687. (b) Espinsosa-Garcia, J.; Corchado, J. R. *J. Phys. Chem.* **1997**, *101*, 7336.
(25) Nizamov, B.; Setser, D. W.; Wang, H.; Peslherge, G. H.; Hase, W. L. *J. Chem. Phys.* **1996**, *105*, 9897.
(26) (a) Martell, J. M.; Mehta, A. K.; Pacey, P. D.; Boyd, R. J. *J. Phys. Chem.* **1995**, 99, 8661. (b) Sekusak, S.; Liedl, K. R.; Rode, B. M.; Sabljic, A. *J. Phys. Chem*. **1997**, *101*, 4245. (c) Hu, W.-P.; Rossi, I.; Corchado, J. C.; Truhlar, D. G. *J. Phys. Chem*. **1997**, *101*, 6911. (d) Steckler, R.; Thurman, G. M.; Watts, J. D.; Bartlett, R. J. *J. Chem. Phys*. **1997**, *106*, 3926. (e) Nyman, G. *J. Chem. Phys*. **1996**, *104*, 6154. (f) Nyman, G.; Clary, D. C. *J. Chem. Phys.* **1994**, *101*, 5756.
(27) Barone, S. B.; Turnipseed, A. A.; Ravishankara, A. R. *J. Phys. Chem*. **1996**, *100*, 14694, 14703.
(28) (a) McKee, M. L. *J. Phys. Chem*. **1993**, *97*, 10971. (b) Muiño, P. Private communication, 1999.
(29) Stutz, J.; Ezell, M. J.; Finlayson-Pitts, B. J. *J. Phys. Chem.* **1987**, *101*, 9187.
(30) Papineau, N.; Flaud, J.-M.; Camy-Peyret, C.; Guelachvili, G. *J. Mol. Spectrosc*. **1981**, *87*, 219.
(31) Flaud, J.-M.; Camy-Peyret, C. *J. Mol. Spectrosc*. **1975**, *55*, 278.
(32) Clough, S. A.; Beers, Y.; Klein, G. P.; Rothman, L. S. *J. Chem. Phys*. **1973**, *59*, 2254.
(33) Camy-Peyret, C.; Flaud, J.-M. *Mol. Phys.* **1976**, *32*, 523.
(34) Rothman, L. S.; Gamache, R. R.; Tipping, R. H.; Rinsland, C. P.; Smith, M. A. H.; Benner, D. C.; Devi, V. M.; Flaud, J.-M.; Camy-Peyret, C.; Perrin, A.; Goldman, A.; Massie, S. T.; Brown, L. R.; Toth, R. A. *J. Quantum Spectrosc. Radiat. Transfer* **1992**, *48*, 469.